NASA Technical Memorandum 86714

Recent Developments in Rotary-Balance Testing of Fighter Aircraft Configurations at NASA Ames Research Center

Gerald N. Malcolm and Lewis B. Schiff

July 1985

Recent Developments in Rotary-Balance Testing of Fighter Aircraft Configurations at NASA Ames Research Center

Gerald N. Malcolm and Lewis B. Schiff, Ames Research Center, Moffett Field, California

July 1985

NASA

National Aeronautics and
Space Administration

Ames Research Center
Moffett Field, California 94035

RECENT DEVELOPMENTS IN ROTARY-BALANCE TESTING OF FIGHTER AIRCRAFT
CONFIGURATIONS AT NASA AMES RESEARCH CENTER

Gerald N. Malcolm and Lewis B. Schiff
NASA Ames Research Center, Moffett Field, California

SUMMARY

NASA Ames Research Center has an ongoing research program to investigate high-angle-of-attack aerodynamic phenomena associated with high-performance aircraft. As part of this research effort, two rotary-balance apparatuses have recently been developed for testing airplane models in a coning motion. A new large-scale apparatus, developed for use in the 12-Foot Pressure Wind Tunnel primarily to permit testing at high Reynolds numbers, was recently used to investigate the aerodynamics of a 0.05-scale model of the F-15 fighter aircraft. Effects of Reynolds number, spin-rate parameter, model attitude, presence of a nose boom, and model/sting mounting angle were investigated.

A smaller apparatus, which is a modernized version of a coning rig developed several years ago to investigate the aerodynamics of bodies of revolution in a coning motion, has been used in the 6- by 6-Foot Supersonic Wind Tunnel to investigate the aerodynamic behavior of a simple representation of a modern fighter, the Standard Dynamics Model (SDM). Effects of spin-rate parameter and model attitude were investigated. This paper presents a description of the two rigs and a discussion of some of the results obtained in the respective tests.

SYMBOLS

A   reference area, F-15 (0.1472 m^2, 1.52 ft^2), SDM (0.0174 m^2, 0.187 ft^2)

b   wingspan, F-15 (0.652 m, 2.14 ft), SDM (0.2286 m, 0.75 ft)

$\bar{c}$ wing mean aerodynamic chord, F-15 (0.243 m, 0.797 ft), SDM (0.0862 m, 0.283 ft)

C_A axial force/qA

C_ℓ rolling moment/qAb

C_{ℓ_ω} $dC\ell/d(\omega b/2V)$, slope of rolling moment coefficient versus $\omega b/2V$ at $\omega = 0$

C_m pitching moment/$qA\bar{c}$ (center of moment at 0.25 $\bar{c}$)

C_n yawing moment/qAb (center of moment at 0.25 $\bar{c}$)

C_{n_ω} $dCn/d(\omega b/2V)$, slope of yawing moment coefficient versus $\omega b/2V$ at $\omega = 0$

C_N normal force/qA

C_Y side force/qA

M   free-stream Mach number

q   free-stream dynamic pressure

R   Reynolds number based on $\bar{c}$

V   free-stream velocity

α angle of attack

α_s sting angle (Fig. 4)

β angle of sideslip

$\phi_{1,2,3}$ rotational position axes (Fig. 3)

ω angular velocity of rotary apparatus about the wind axis

Note that force and moment coefficients are with respect to body-fixed axes.

1. INTRODUCTION

NASA Ames Research Center sponsors a research program to understand and exploit the aerodynamic phenomena which occur on high-performance fighter aircraft, particularly at high angles of attack. A number of facets comprise this research program, including fundamental fluid-mechanics studies, derivation and verification of aerodynamic mathematical models, assessment of the aerodynamics effects on flight dynamics, and the development of new test apparatuses for performing the necessary wind-tunnel experiments.

One of the required experiments is to measure the aerodynamic properties of a vehicle in a continuous spin motion about the velocity vector, sometimes referred to as a coning motion. This experiment can be performed with a rotary-balance apparatus or, simply, a rotary rig. Rotary rigs have been developed in the United States and a number of other countries in the past few years. Some of these rigs have been described in a recent AGARD lecture series (Ref. 1).

Two rotary rigs have been developed at NASA Ames Research Center. The first rig to be discussed is a large-scale apparatus for testing airplane configurations in the Ames 12-Foot Pressure Wind Tunnel. This rig was developed to provide a capability for high-Reynolds-number rotary-balance tests. A preliminary report on the development of this rig is given in Ref. 2. The first wind-tunnel test using this rig was recently completed on a 0.05-scale model of the F-15 fighter aircraft. Availability of flight-test data from NASA Dryden Research Facility was the main reason for choosing the F-15 configuration. The flight tests were conducted on a 0.375-scale F-15 Spin Research Vehicle (SRV) and provided extensive data on steady and nearly steady spins. Although this paper addresses only the wind-tunnel test apparatus and data, a long-term objective of the research program is to compare wind-tunnel and flight-test data for steady spin cases.

The second rig is a small-scale rotary rig that was originally constructed for tests on bodies of revolution in the Ames 6- by 6-Foot Supersonic Wind Tunnel (Ref. 3), and later was modified for exploratory tests in the 12-foot tunnel (Refs. 4 and 5) on simple airplane configurations. This rig has recently been refurbished with a new hydraulic drive system and associated hardware and a modern control system. The first test of this apparatus was recently completed in the Ames 6- by 6-foot tunnel using a simplified version of a modern fighter aircraft, referred to as the Standard Dynamics Model (SDM).

This paper is a report of recent progress in the development and use of rotary rigs at NASA Ames. Some examples of data recently obtained on both apparatuses are presented. The details of each apparatus are addressed in Section 2. Similarly, the results of the individual wind-tunnel experiments are discussed in Section 5. Both rigs use a common data-acquisition system and share a common data-reduction technique, and they are discussed in Sections 3 and 4.

2. DESCRIPTION OF WIND-TUNNEL FACILITIES AND APPARATUSES

2.1 12-Foot Pressure Wind Tunnel Apparatus

The objectives for the first test of this apparatus in the tunnel were three-fold. The first was to install and check the apparatus and all associated equipment and instrumentation in the wind-tunnel environment. The second was to acquire aerodynamic data on a fighter aircraft model in a spin motion at various attitudes (α = -5° to 90°, β = -15° to +15°) at Reynolds numbers ranging from 1 to 5.5 million based on wing mean aerodynamic chord. The third was to acquire wind-tunnel data that could be used for comparison with the Dryden SRV flight-test data. Since the SRV had a rather large nose boom to measure model attitude and speed in flight, the wind-tunnel model was tested both with and without a nose boom.

2.1.1 12-Foot Pressure Wind Tunnel

The 12-Foot Pressure Wind Tunnel is a variable-pressure, low-turbulence facility with a total pressure capability range of 5.0 atm. Mach number can be varied from 0.1 to 0.98; however, because of the solid-wall test section and limited power, operation of the tunnel beyond a Mach number of 0.5 yields questionable results. A unit Reynolds number up to approximately 25 million/m can be obtained at M = 0.28.

2.1.2 Apparatus and Model

The rotary apparatus and the model with the nose boom attached are shown installed on a laboratory test stand in Fig. 1. A protective enclosure surrounds the apparatus for safety purposes while it is rotating. The rig and model (minus the nose boom) installed in the 12-foot tunnel test section are shown in Fig. 2. A sketch of the apparatus is shown in Fig. 3. For efficient operation in a pressure tunnel, it is essential to minimize the number of tunnel startups and shutdowns necessary to change model attitude. To accomplish this, the rig was designed with electrically driven movable arms which permit remote change of the angles of attack and sideslip. The desired angles are obtained by rotating two arms on the rig (while it is stationary) about the axes ϕ_1 and ϕ_2 as shown in Fig. 3. These axes intersect the spin axis at the designated longitudinal location on the model representing the center of gravity of a full-scale, free-flying vehicle. By using a straight, base-mounted sting, the angle of incidence of the model with respect to the flow can be varied from -30 to 30°. By top-mounting the model on bent stings (α_s = 45° and 70°), the angles of attack and sideslip can be varied over the envelope shown in Fig. 4 (α from -30° to +100° with β between ±30°). Figure 5 shows a photograph of the model mounted on each of the three stings. A remotely

2

driven counterweight (Figs. 1-3) was positioned to statically balance the mass distribution of the system about the spin axis prior to rotating the rig. Potentiometers mounted on the arms gave remote indications of the positions of the arms and of the counterweight position.

The apparatus is rotated about an axis parallel to the wind-tunnel airstream at speeds ranging from 0 to 37 rad/sec (0-350 rpm) in either a clockwise or counterclockwise direction using a servo-controlled hydraulic drive system. No attempt was made to dynamically balance the system. The magnitude of the centrifugally induced dynamic moment was, in the worst case, as much as 45,200 N·m (400,000 in.-lb). Because of the large dynamic loads experienced by the fixed part of the rotary rig and the tunnel support system, special provisions were made to secure the system as rigidly as possible. The center body of the support system is normally traversed and pitched on the vertical blade strut to vary the model attitude. For this test, the center body was rigidly fastened to the strut with threaded pins to prevent any motion between the rig/centerbody and the tunnel strut. To eliminate possible resonance of the rotary-apparatus/tunnel support system, it was designed to have a natural frequency at least three times the maximum rotational frequency of 37 rad/sec.

The model is a 0.05-scale version of an F-15 fighter configuration with two nose configurations available, one with a nose boom and one without. The center of moments is at 0.25 of the mean aerodynamic chord of the wing. This location is also the center of rotation of the model about the spin axis. Control deflections can be changed manually. The horizontal tails can be varied at any desired angle in 5° increments. The aileron and rudder surfaces can be set at 0° or at the maximum angles of ±20° for the ailerons and ±30° for the rudders.

The forces and moments are measured using a 5.08-cm (2 in.) diameter, six-component, strain gage balance mounted in the model. Since the spin axis of the rig is parallel to the wind stream, constant angles of attack and sideslip are maintained during a rotation cycle. Thus, the resulting balance output is constant at any given rotational speed, except for cyclical variations due to model weight and aerodynamically induced unsteadiness. The one-piece balance, constructed especially for use with this apparatus and model, can be attached to the sting through the rear or the top of the model. Electrical power and signal paths from the balance are provided by a slip-ring assembly mounted in the circular housing near the strut mount. The slip-ring assembly also carries the power leads to the electrically driven movable arms and the signals from the arm-position potentiometers. A resolver is mounted on the rear of the slip-ring unit to measure the angular position of the rig about the spin axis. A tachometer to determine spin rate is mounted on the hydraulic drive motor shaft.

Because of the extremely large centrifugally induced oscillatory loads on the apparatus and the tunnel support system (caused by the large dynamic imbalance of the rig), an extensive amount of data was collected continuously during the test to monitor the structural integrity of the apparatus and support. Numerous locations on the apparatus and the tunnel support system were instrumented with strain gages to monitor stresses, eddy-current proximity probes to measure deflections, and accelerometers to measure the vibration amplitudes and frequencies. In addition, pressure instrumentation was used to monitor the important pressures within the hydraulic drive system. Although essential to safe operation of the apparatus, the monitoring instrumentation is not discussed further in this paper.

2.2 6- by 6-Foot Supersonic Wind Tunnel Apparatus

2.2.1 6- by 6-Foot Supersonic Wind Tunnel

The 6- by 6-Foot Supersonic Wind Tunnel is a variable-pressure tunnel with a total pressure range of 0.3 to 1.0 atm. The Mach number can be varied from 0.25 to 2.2 continuously. Reynolds numbers to 15×10^6/m can be achieved. The tunnel has an asymmetric sliding-block nozzle for changing Mach number and a test section with perforated floor and ceiling to permit testing at transonic Mach numbers.

2.2.2 Apparatus and Model

Figure 6 is a diagram of the small-scale rotary-balance apparatus. A hydraulic motor is used to turn a shaft aligned nominally parallel to the wind-tunnel airstream. Any one of a series of interchangeable bent stings can be attached to the rotating shaft to vary the angle of incidence with respect to the airstream. The stings are designed to support a model on a strain-gage balance at pitch angles ranging from 0 to 30° while keeping the same axial model station on the axis of rotation. The rig follows the same basic concept, and uses the same bent stings, as an earlier rotary-balance apparatus (described in Ref. 3), but it is considerably more sophisticated in that it uses speed and position sensors and the corresponding feedback control loops (similar to those of the 12-ft tunnel apparatus) to give the operator close control of either the speed or angular position of the rotating shaft.

The balance used was a standard six-component Task Corporation 3.81 cm (1.5 in.) diameter MK XIXA balance, with all power and signal lines routed through the bent sting and the shaft of the hydraulic motor. A set of gold slip rings and brushes was used to transfer the signals to the nonrotating portion of the rig. Model attitude was set by adjustment of the pitch and roll angles of the model. Pitch angles were determined by the choice of bent sting, and roll angles by choice of a fixture located between the balance and the model which maintained a set roll angle. A set of such roll fixtures was available, including one for use with all bent stings giving zero sideslip angle, and one for each of the bent stings to obtain sideslip angles of either -5° or +5°.

3

The rig is capable of being driven at rotation rates from 0 to 63 rad/sec (600 rpm) in either direction. Since the rotating parts are neither statically nor dynamically balanced, the centrifugally induced oscillatory loads generated on the nonrotating structure at maximum rotation rate are quite large. The rig is designed to withstand these loads, but some additional measures were necessary to prevent excessive deflection of the rig support structure in the tunnel. The tunnel's body of revolution, which is vertically supported by lead screws and laterally restrained by rollers, was clamped rigidly to the vertical strut in this case. Brass pads were installed between the body of revolution and the vertical strut to distribute the load and prevent damage to the strut surface. In addition, a pair of diagonal braces, extending from the leading edge of the vertical strut to the tunnel floor, was installed to restrain lateral movement of the rig support. Vibration amplitudes, in both vertical and lateral planes, were monitored by accelerometers mounted on the body of revolution, and these confirmed that no excessive vibration levels occurred while the rig was running.

An additional feature of the rotary rig is the camera enclosure shown in Fig. 6. This is capable of holding a miniature video or movie camera, with power and signal lines routed through the previously mentioned slip ring set. The camera views the upper surface of the model, and since the camera and model rotate together the model image remains steady regardless of the motion of the rig. This feature was included to enable vapor-screen investigations of the behavior of the vortex wake of the model in response to coning motion.

Figure 7 is a photograph of the model (designated the Standard Dynamics Model, SDM) used in this investigation. The basic planform is that of a current high-performance aircraft configuration. It was deliberately designed for manufacture by simple machining techniques to encourage its widespread use as a standard model for testing in different wind tunnels and on different dynamic test rigs. The model was designed and manufactured by the National Aeronautical Establishment (NAE), Canada. A more complete description of its geometry and characteristics is contained in Refs. 6 and 7. The center of moments was located at 0.35 of the wing mean aerodynamic chord, which was coincident with the center of rotation of the model about the spin axis.

3. DATA ACQUISITION AND REDUCTION SYSTEM

The data for both rotary-balance apparatuses were taken and reduced with a common stand-alone microcomputer system. Conventional analog signal-conditioning equipment was used to process and filter the balance and tachometer signals. Low-pass filtering of the balance signals eliminated the oscillatory signals due to model weight. A special data-acquisition unit processed the signals from the balance, shaft tachometer, rig angular position encoder, and (in the case of the 12-ft tunnel apparatus) the arm-position potentiometers. Tunnel conditions, including tunnel temperature and pressures, were routed to the system by paralleling the conventional tunnel sensors.

In addition to the data-acquisition unit and the main central processing unit, the data system included a dual floppy disk drive, external printer, and a multicolor on-line plotter. The data system provided complete on-line listings and plots of the six force and moment coefficients as a function of the apparatus spin rate.

4. ROTARY AND STATIONARY TARE MEASUREMENTS

There are three types of forces and moments acting on the balance when the apparatus and model are rotated in the wind tunnel. The first are the inertial forces and moments due to the moments of inertia of the rotating model. These vary with model attitude and rotation speed, and may be compensated for by measuring wind-off rotating tares and subtracting them from the wind-on data. The second are oscillatory forces caused by the change in orientation of the model mass relative to gravity. Although it is possible to account for these forces analytically, they were eliminated in a more straightforward manner by low-pass filtering the balance signals. The remaining forces and moments are the aerodynamic loads of interest.

The magnitude of the inertial loads can be calculated in a straightforward manner if the moments of inertia about the principal axes of the model and the location of the model center of mass with respect to the rotation axis are known and do not vary with rotation rate. However, the model/sting combination deflects during rotation, and will cause the actual inertial loads to vary from the analytically determined values. Therefore, it is necessary to measure wind-off tare loads at the model attitude and rotation rates planned for the wind-on tests. These measurements are stored in the data-acquisition system and later subtracted from the wind-on measurements.

For accuracy, the inertial tare loads should be measured with the model either in a complete vacuum or surrounded by an enclosure that rotates with it. This will prevent any interaction of the surrounding still air with the model as it rotates. However, in some cases, depending on such factors as model size, rotation rates, and expected wind-on loads, the contribution from this effect can be ignored. In these tests, the tare values measured in the clockwise and counterclockwise directions were averaged. For the case where the sideslip angle is set to zero, the effects of the surrounding air on side force, yawing moment, and rolling moment should be equal and opposite in sign. In this case, averaging the measured values is nearly the same as measuring the tares in a vacuum. However, the effects on normal force, pitching moment, and axial force are not eliminated by averaging the measurements from both rotational directions. It is felt that the

4

still-air loads are small enough to ignore, particularly for these experiments where the inertial loads and the air loads are very large in comparison.

Typically, wind-off forces and moments were determined at several fixed rotation rates ranging from 0 to the maximum for each rotary rig. The respective forces and moments were fit with a five-term polynomial of the form

$$F = A_0 + A_1\omega + A_2\omega^2 + A_3\omega^3 + A_4\omega^4$$

where F is the force or moment and ω is the rotation rate. The coefficients A_0 through A_4 were then stored. The same procedure was used for rotation in the opposite direction. The two sets of coefficients were then averaged to create a combined tare file of one set of coefficients that was applicable to all rotation rates for that particular angle of attack and sideslip.

The original intent was to measure all the rotating tare loads in the laboratory prior to installing the apparatus in the tunnel, and store them for later use during the tunnel test. The purpose was to eliminate the expenditure of valuable tunnel occupancy time to perform the tare measurements. Tares were, in fact, measured prior to tunnel installation, but it was soon recognized, after repeating some tare measurements in the tunnel, that there was enough variation in the measurements (when compared to those previously acquired in the laboratory) that new tares would have to be measured in the tunnel. The discrepancy was caused by a small difference between the stiffness of the support systems in the tunnel and the laboratory which resulted in a difference in the deflection of the model center of mass relative to the rotation axis for the two support systems.

An additional effect of deflection is the change in position of the model with respect to the rotation axis caused by the wind-on load as compared to the wind-off condition. This effect cannot easily be accounted for and, since it was felt to be small, no attempt was made to correct the wind-on data.

When data are taken with the model stationary ($\omega = 0$) in the wind tunnel with the wind on, the weight of the model must be accounted for. (For the case where the model is rotating, the weight is averaged to zero over a cycle by using low-pass analog filters.) Model weight is accounted for by performing a series of wind-off static tare measurements at various known angular positions around the rotation axis and determining the weight effect on the balance. The weight component on the balance with the wind on is then calculated, using the angular position of the rig with respect to the tunnel and the attitude of the model with respect to the rig.

5.   EXPERIMENTAL RESULTS

5.1   12-Foot Tunnel Experiments

The effects of a number of variables on the aerodynamics were examined during this experiment. Included are variations in Reynolds number, angles of attack and sideslip, sting angle, and the presence of a nose boom. A Mach number of 0.28 was selected for the majority of the tests, since this maximizes the Reynolds number capability of the tunnel. Later in the test program, in order to obtain larger values of the spin-rate parameter $\omega b/2V$ (where b is the span and V the tunnel free-stream velocity), some runs were conducted at a decreased velocity resulting in a decrease of the Mach number to 0.2. Comparisons between the results measured at Mach   and 0.28 indicated that effects due to the change in Mach number were negligible. The aerodynamic coefficients determined included: normal force, pitching moment, side force, yawing moment, and rolling moments. Axial force was also measured, but it was not determined with accuracy comparable to the other components, nor was it felt to be particularly important for these tests. The following discussion will introduce some examples of the data obtained during this test and will highlight some of the more interesting results.

5.1.1   Static Aerodynamic Data

The variations of the normal-force and pitching-moment coefficients with angle of attack are shown for the configuration without the nose boom in Fig. 8. Results are shown for Reynolds numbers of 1.5 million and for 4.0 or 5.5 million. Also shown for comparison are the data obtained at much lower Reynolds numbers (0.2 million) on a rotary rig in the NASA Langley Research Center spin tunnel (Ref. 8). As explained earlier in the description of the apparatus, data were acquired with three different stings but at some angles of attack there is an overlap of the data. For example, data were obtained at $\alpha = 30°$ on both the straight base-mounted sting and the top-mounted 45° sting. Between α of 50° and 70° data were obtained on both the 45° and 70° stings. The overlapping sets of data are shown in Fig. 8. As can be seen from Fig. 8, the normal-force coefficient peaks between α of 35° and 40° and remains almost constant for 40° $\leq \alpha \leq$ 90°, except for a slight decrease between α of 50° and 60°. There is some variation with Reynolds number and, interestingly, the trend in direction with Reynolds number is consistent with the data from the Langley rotary rig. There are noticeable differences, as well, due to the different sting angles. The moment center for the pitching-moment coefficient data is the 0.25 position of the wing mean aerodynamic chord. The variation with Reynolds number is primarily caused by the behavior of the flow over the forebody and fuselage and not by variations of the flow over the wing and tail surfaces. This is particularly true at the higher angles of attack since the flow almost assuredly separates at the wing leading edge regardless of the Reynolds number. Conversely, the flow separation around the forebody and the rounded

corners of the inlets, and the resulting variation of the forces and moments, are known to be sensitive to Reynolds number.

The variation of the yawing- and rolling-moment coefficients with angle of attack, for a range of Reynolds numbers, is shown in Fig. 9 for the configuration without the nose boom. There is little effect of Reynolds number variation on the yawing-moment coefficient for $\alpha \leq 40°$, and very little effect on the rolling-moment coefficient at all angles of attack. At angles of attack where significant crossflow separation exists, Reynolds number variation mainly affects the flow over the forebody and the fuselage. The resulting differences in the forces and moments would be expected primarily in the yawing moment. In addition, the effects of different sting angles are also sizable, particularly at $R = 1.5$ million. The primary effect of changing the sting angle is to influence the leeward flow field and the resulting interaction of the leeside vortices over the fuselage and vertical and horizontal tail surfaces. Many of the studies that have been done to investigate the asymmetric vortex phenomena on ogive-cylinder bodies at high angles of attack have shown that the maximum asymmetry and resulting values of side force and yawing moment occur between α of 50° and 70°. The results of this experiment are consistent with that observation. There appears to be a slight bias in the direction of the rolling-moment coefficient at all angles of attack although the sideslip is supposedly zero. It is possible that there is a slight asymmetry in the model or perhaps a very small sideslip angle caused by misalignment of the model in the airstream.

A similar presentation of the yawing- and rolling-moment data is shown in Fig. 10 for the model with the nose boom installed. Again, the variation with Reynolds number is fairly significant for angles of attack greater than 40°. Even more interesting, however, is the change in the coefficients, particularly the yawing-moment coefficient, when compared to the boom-off case shown in Fig. 9. At higher angles of attack, the presence of the nose boom can significantly alter the vortex flow field on the forebody and noticeably influence the resulting moments. For example, at $\alpha = 60°$ with a sting angle of 45°, the yawing moment shown in Fig. 10 at $R = 4.0$ million has the opposite sign to that shown in Fig. 9. However, it is also apparent that the sting angle has a major influence on the result. This can be seen by comparing the data at $\alpha = 60°$ and $R = 4.0$ million for sting angles of 45° and 70° (Fig. 10).

The implication of the results shown are certainly of some concern for determining the aerodynamics of configurations at high angles of attack. The differences caused by the presence of a nose boom illustrate the sensitivity of the aerodynamics to the forebody configuration. Since many flight-test aircraft employ a nose boom to acquire air data, there can be significant differences between the aerodynamics of the flight-test aircraft and the operational aircraft which, typically, do not have a nose boom. The differences observed due to the sting angle also illustrate the problems of supporting a model in a wind tunnel at large incidences without altering the leeward-side flow field.

5.1.2 Rotary Aerodynamic Data

The data in this section are shown as variations of yawing-moment and rolling-moment coefficients with the nondimensional rotation rate or spin-rate parameter, $\omega b/2V$. Figure 11 shows results for angles of attack from 0° to 90° and a Reynolds number of 1.5 million for the configuration without the nose boom. For angles of attack ranging from 0° to 40°, the variation of C_n with spin rate is reasonably linear. Above $\alpha = 40°$ the behavior is fairly nonlinear, and for the case of $\alpha = 60°$, there is a sizable offset in the yawing-moment at zero rotation rate. In all cases the overall slopes of the C_n curves exhibit an anti-spin behavior. Despite this, the offset in the nonrotating value of the yawing-moment coefficient at $\alpha = 60°$ causes a significant pro-spin tendency for all values of $\omega b/2V$ less than zero. The behavior of the rolling-moment coefficient with increasing angle of attack is worth examining. The rolling moment is anti-spin for angles of attack up to 20°, but for α from 25° to 40° and for α of 80° to 90°, the rolling moment is generally pro-spin. Figure 12 shows similar results for Reynolds numbers of 4.0 and 5.6 million. Comparing the results to those shown in Fig. 11, some differences are observed due to Reynolds number variation, particularly at angles of attack above 30°.

Figures 13-15 show the yawing-moment coefficient for angles of attack of 30°, 50°, and 70°, respectively, for the model with and without the nose boom. The different curves compare results obtained at high and low Reynolds numbers for a given sting angle, and for results obtained with different sting angles at the same Reynolds number. Figure 13, for $\alpha = 30°$, shows linear behavior of the moment with the spin-rate parameter for both the boom-off and boom-on configurations. Some differences due to Reynolds number can be observed at the higher rotation rates, especially for the case with the boom on. There is a slight effect of sting angle on the data as well, primarily at the higher rotation rates. Similar data obtained for $\alpha = 50°$ are shown in Fig. 14. The results, in general, show a higher degree of nonlinearity than for $\alpha = 30°$.

The most interesting case is shown in Fig. 15 for $\alpha = 70°$. Looking first at the configuration without the nose boom in Fig. 15a, there is very little effect of the sting angle at the higher Reynolds number. However, at the lower Reynolds number, a significant effect of the sting angle is observed at the higher rotation rates. There is also a considerable difference between the results obtained for the two Reynolds numbers using the same sting.

The effects of adding the nose boom at this angle of attack are rather dramatic, as seen in Fig. 15b. The first characteristic to note is that the data obtained with the 70° sting at $R = 1.5$ million (circles) show a yawing-moment coefficient that is multivalued over a wide range of values of the spin-rate parameter. This multivalued variation and the accompanying hysteresis loop indicate that two flow field states

6

can exist around the model for a given spin rate. Which of the two possible states that can exist depends on the past history of the flow, that is, whether that spin rate is approached from a rate that is higher or lower. (A description of the hysteresis loop and details of the dependence of its characteristics on Reynolds number are discussed later in this section in connection with Fig. 16.) The hysteresis effect is quite sensitive to model support interference. Although two flow states are also evident for the results obtained using the 45° sting at R = 1.5 million, the hysteresis is almost negligible. This difference in hysteresis effect and the large difference between yawing-moment coefficient values at negative spin rates demonstrate the sensitivity of the aerodynamics to sting angle differences and resulting support interference effects. It is apparent from these results that there is a sizable influence of the two stings on the leeward flow field which, in turn, affects the yawing moment. For the measurements made at α = 70°, the 70° sting is parallel to the tunnel airstream. Conversely, for α = 70°, the 45° sting is inclined with respect to the airstream and probably creates more of a disturbance in its wake, thus influencing the flow field more severely. At the higher Reynolds number, 4.0 million, no hysteresis was observed in the measurements made with either sting, and the results obtained with both stings are in reasonably close agreement.

Figure 16 illustrates, in more detail than Fig. 15b, the effect of Reynolds number variation on the yawing-moment coefficient versus the spin-rate parameter. The case shown is for α = 70°, α_s = 70°, and Reynolds numbers ranging from 1.0 million to 4.0 million. The most obvious effect of Reynolds number variation is the change in the value of the spin-rate parameter at which a "jump" in the yawing-moment coefficient occurs, caused by switching from one flow state to another. At R = 1.0 million there is no jump or significant hysteresis except for a small hysteresis loop at the larger positive values of the spin-rate parameter. At a slightly larger Reynolds number, 1.2 million, the jump occurs at a value of ωb/2V near -0.08. With further increase in Reynolds number, to 1.3 million, the jump point is observed at a value of spin-rate parameter near -0.04. A small hysteresis loop is observed in both these cases surrounding the jump condition. For R = 1.3 million it is interesting to note that the first jump (indicated by a (1) on the curves) occurs at ωb/2V = -0.01. The flow was relatively unstable and soon returned to the original state (2) until the spin-rate parameter reached -0.04, where the moment jumped again (3). With an increase in Reynolds number to 1.5 million, the yawing-moment coefficient becomes multivalued, as described previously in Fig. 15b, and significant hysteresis loops are observed. The following describes the sequence of acquiring the data in the hysteresis loop.

For the case shown at R = 1.5 million, the initial value of the yawing-moment coefficient was negative. The initial rotation direction was in the negative direction, and the yawing-moment coefficient remained negative until ωb/2V = -0.036, then it jumped to a positive value (1). The moment remained positive as the rotation rate was slowly increased in the negative direction to ωb/2V = -0.12. The rotation rate was then slowly decreased to zero and increased in the opposite or positive direction. The corresponding yawing-moment coefficient response remained positive until the model reached a value of spin-rate parameter of 0.09 then jumped (2) to a negative value. As the spin-rate parameter was slowly increased to its maximum value and then decreased through zero, the yawing-moment coefficient again jumped to a positive value as ωb/2V decreased through -0.03 (3). However, as the spin-rate parameter was decreased to its maximum negative value and then increased through zero for the second time, the jump in the yawing-moment coefficient to a negative value occurred at ωb/2V = 0.01 (4) rather than at ωb/2V = 0.09 as before. It is apparent, following this path as shown, that there is hysteresis in the value of the yawing-moment coefficient with variation of the spin-rate parameter. This type of variation indicates the dependency of the flow field asymmetry, not only on the direction of rotation, but on the history of the rotation direction. It is interesting that this characteristic of a multivalued yawing-moment coefficient was observed only at this angle of attack and a small range of Reynolds numbers on the configuration with the nose boom. Repeated runs at these same conditions produced essentially the same results with only a small variation in the value of ωb/2V where the jumps occurred. The repeatability of the jump condition is very sensitive to the Reynolds number.

Data obtained for R = 2.4 million and R = 4.0 million do not indicate two flow states and are essentially single-valued. The only exception is observed at the extreme negative values of ωb/2V. The variation is relatively linear and, for the highest Reynolds number, R = 4.0 million, there is little offset in the yawing-moment coefficient at zero spin rate. At the higher Reynolds numbers the flow on the forebody and inlet surfaces is likely to be turbulent, and the flow separation is not as sensitive to the rotation-induced local flow angularity.

The effect of variation of sideslip angle on the hysteresis is illustrated in Fig. 17. Data are shown for R = 1.5 million at α = 70° for the boom-on configuration, with β ranging from -5° to +10°. At β = 5° and β = -5° the jumps in the yawing-moment coefficient occur at values of spin-rate parameter on either side of the value at which the jump was observed at β = 0°. For β = 10°, the flow angularity on the model resulting from the combination of sideslip and rotation angles is apparently not sufficient to cause a jump in the flow orientation as seen in the other cases. For comparison, the data are shown for the model without a nose boom at β = 0° at the same conditions. As seen in Fig. 15a, there is little indication of asymmetry, which is a significant contrast to the data obtained with nose boom on.

5.2 6- by 6-Foot Tunnel Experiments

The tests conducted on the SDM in the 6- by 6-ft tunnel were all performed at Mach 0.6 and a Reynolds number of 0.88 million based on the wing mean aerodynamic chord. These test conditions were chosen to match those of complementary forced-oscillation tests performed at the NAE (Refs. 6 and 7). The aerodynamic coefficients measured in the 6- by 6-ft tunnel and reported in Ref. 9 included normal force, pitching

moment, side force, yawing moment, rolling moment and axial force. The model center of rotation was located at 0.35 of the wing mean aerodynamic chord. This point was also chosen as the moment reference center. Some of the results obtained will be presented in the following sections.

5.2.1 Rotary Aerodynamic Data

Some results will be shown in this section to illustrate the variation of the aerodynamic coefficients with the spin-rate parameter, $\omega b/2V$. Figure 18a shows the force and moment coefficients measured at $\beta = 0°$, $\alpha = 10°$. Similar results obtained at $\beta = 0°$ and $\alpha = 30°$ are shown in Fig. 18b. Note that although data were taken at zero spin rate, they have not been included in Fig. 18 because a small misalignment between the rotary rig spin axis and the local free-stream direction made these static data dependent on the angular position of the rig. However, with the rig rotating, low-pass filtering of the data signals effectively averaged out the effect of flow angularity.

At zero angle of sideslip, symmetry conditions dictate that the lateral aerodynamic coefficients (C_Y, C_n, and C_ℓ) should be odd functions of the spin-rate parameter, while the longitudinal aerodynamic coefficients (C_N, C_A, and C_m) should be even functions of the spin rate. This is demonstrated by the data presented in Fig. 18. For all angles of attack tested, the lateral aerodynamic coefficients were observed to be nearly linear with respect to spin-rate parameter over the range of spin rates achieved in the test. The longitudinal aerodynamic coefficients were seen to be even functions of the spin-rate parameter. At the lower angles of attack, characterized by the results shown for $\alpha = 10°$ in Fig. 18a, the longitudinal aerodynamic coefficients are almost independent of spin rate. At the higher angles of attack, typified by the results shown for $\alpha = 30°$ in Fig. 18b, the axial-force and pitching-moment coefficients show a parabolic variation in spin-rate parameter rate. Some of this parabolic variation is undoubtedly real, and is probably caused by increased velocities and dynamic pressure on the tail resulting from the coning motion, which produces increased tail lift. However, limitations of data resolution at these low levels of C_A and C_m, and in particular the choice of the moment center position, may also be responsible for exaggerating the scale of the variation.

The effects of variation of sideslip angle are shown in Fig. 19, which presents data obtained at $\beta = -5°$ and $\beta = +5°$. Figure 19a shows data obtained at $\alpha = 9°$, while corresponding data measured with $\alpha = 30°$ are shown in Fig. 19b. Once again, the linear variation of the lateral aerodynamic coefficients with spin-rate parameter is apparent. The nonlinear variation of the longitudinal aerodynamic coefficients with spin rate is also apparent. The longitudinal aerodynamics also show an effect due to sideslip, which, as expected, introduces a reasonably symmetric and linear component with spin-rate parameter. In general, the results show a reasonable symmetry with direction of sideslip, but with some offsets possibly introduced by small asymmetries in the model and/or the effects of combined centrifugal and aerodynamic loading.

5.2.2 Static Aerodynamic Data

Static aerodynamic data are presented in Figs. 20 and 21. These data were obtained from the intercepts, at $\omega = 0$, of the low-spin-rate data analogous to that presented in Figs. 18 and 19. The actual static data taken at $\omega = 0$ were not used because of the scatter caused by flow angularity relative to the rotary rig's axis of rotation.

The effects of variations in the angle of attack and sideslip on the normal-force and pitching-moment coefficients are shown in Fig. 20, while the corresponding effects on the yawing-moment and rolling-moment coefficients are presented in Fig. 21. Also shown are the static data given in Ref. 6, obtained at the NAE using the same model on a similarly sized sting support. In most respects the two sets of data are well-matched, with the exception of the normal-force and pitching-moment coefficients measured at the larger angles of attack. It is suggested that this discrepancy is probably attributable to wall- and strut-interference effects in the small 0.75 m × 0.38 m solid-wall tunnel used for the NAE tests. Such effects should be negligible for the measurements made in the 6- by 6-ft tunnel, where the blockage based on total planform area of the model and test section cross-sectional area was approximately 1%, and the ratio of wing chord to tunnel test section height was approximately 0.05.

5.2.3 Dynamic Rotary Derivatives

The rotary derivatives presented in Fig. 22 were obtained by least-squares fitting of straight lines through the data presenting the aerodynamic forces and moments as functions of the spin-rate parameter (e.g., Figs. 18 and 19). The derivatives presented in Fig. 22 are the slopes of these lines. The results show a gradual change with angle of attack from 0 to 15°, then a more rapid change as angle of attack reaches and exceeds 20°. In particular, the rolling-moment derivative changes from anti-spin to pro-spin, indicating a significant change in flow characteristics within the angle of attack range from 15° to 20°. This is in agreement with the static aerodynamic data which also show a major change in lateral aerodynamics within the 15° to 20° angle of attack range. In addition, vapor-screen flow visualization studies indicated a major change in the vortices shed from the wing leading-edge strake. At a 15° angle of attack, these vortices passed over the wing surface and remained intact well downstream of the wing trailing edge, but at 20° angle of attack, they burst while still above the wing surface.

6. CONCLUDING REMARKS

As part of an ongoing research program at the NASA Ames Research Center to investigate the aerodynamic phenomena affecting high-incidence flight, two rotary-balance apparatuses have been developed for testing models of airplane configurations in coning motion. The rigs were recently utilized for inaugural tests conducted using a model of the F-15 aircraft in the 12-Foot Pressure Wind Tunnel, and for tests conducted using the Standard Dynamics Model in the 6- by 6-Foot Supersonic Wind Tunnel. Results obtained using both rigs have demonstrated their capabilities as tools for investigating the high-incidence aerodynamics of aircraft at a variety of test conditions.

Tests were conducted in the 12-ft tunnel on a 0.05-scale model of the F-15 airplane, at Mach numbers ranging from 0.2 to 0.28, and at Reynolds numbers, based on wing mean aerodynamic chord, ranging between 1.0 million and 5.5 million. The angles of attack considered ranged from 0 to 90°, with sideslip angles ranging between -15° and +15°. In addition, the effects on the aerodynamics due to the presence or absence of a fuselage nose boom were investigated. Aerodynamic force and moment coefficients were measured at spin rates of up to 350 rpm (nondimensional spin-rate parameter values up to 0.125) in both the clockwise and counterclockwise directions. Some of the main observations from these tests are:

1. Effects of Reynolds number variation generally become significant at angles of attack above 40° and Reynolds numbers below 2.4 million.

2. Variations of the aerodynamic coefficients with spin-rate parameter are nearly linear up to $\alpha = 20°$.

3. Effects of the nose boom are significant at angles of attack above 40°. At $\alpha = 70°$ and $R = 1.5 \times 10^6$, the presence of the nose boom caused major effects on the yawing-moment coefficient. These included the occurrence of multivalued aerodynamic responses, and accompanying aerodynamic hysteresis, over a range of the spin-rate parameter.

4. The effects of sting-support interference can be significant with a top-mounted model, even at large incidence. The angle that the top-mounted sting makes with respect to the model was seen to have a significant effect, particularly at Reynolds number values below 1.5×10^6.

Tests were also conducted in the 6- by 6-ft wind tunnel on the SDM (a simplified generic fighter-aircraft shape) in coning motion at $M = 0.6$, at a Reynolds number, based on wing mean aerodynamic chord, of 0.88 million. The angles of attack considered ranged from 0 to 30°, with sideslip angles ranging between -5° and +5°. These conditions matched those of complementary forced-oscillation tests conducted at the NAE in Canada.

Aerodynamic force and moment coefficients were measured on the SDM at spin rates ranging up to 600 rpm (nondimensional spin-rate parameter values up to 0.04) in both directions. Over the angle-of-attack range investigated, the lateral aerodynamic characteristics show a linear variation over the full range of spin-rate parameters achieved in the tests. Although no discontinuous changes in the aerodynamic characteristics of the SDM were observed with changes in attitude or spin rate, evidence exists of a significant change in flow characteristics between 15° and 20° angles of attack. This is believed to be associated with forward movement of the burst point of the wing strake vortices with increasing incidence; from behind the wing at $\alpha < 15°$, to above the wing at $\alpha > 20°$.

REFERENCES

1. Malcolm, G. N., "Rotary and Magnus Balances," AGARD Lecture Series No. 114, Dynamic Stability Parameters, Paper 6, May 1981, pp. 1-26.

2. Malcolm, G. N., "New Rotation-Balance Apparatus for Measuring Airplane Spin Aerodynamics in the Wind Tunnel," AIAA J. of Aircraft, Vol. 16, No. 4, April 1979, pp. 264-268.

3. Schiff, L. B. and Tobak, M., "Results from a New Wind-Tunnel Apparatus for Studying Coning and Spinning Motions of Bodies of Revolution," AIAA Journal, Vol. 8, No. 11, November 1970, pp. 1953-1957.

4. Clarkson, M. H., Malcolm, G. N., and Chapman, G. T., "Experimental Post-Stall Rotary Aerodynamic Coefficients for Airplane-Like Configurations," AIAA Journal, Vol. 13, No. 8, August 1976, pp. 565-570.

5. Malcolm, G. N. and Clarkson, M. H., "Wind-Tunnel Testing with a Rotary-Balance Apparatus to Simulate Aircraft Spin Motions," Proceedings of AIAA 9th Aerodynamic Testing Conference, Arlington, Texas, June 1976, pp. 143-156.

6. Beyers, M. E. and Moulton, B. E., "Stability Derivatives Due to Oscillations in Roll for the Standard Dynamics Model at Mach 0.6," Report LTR-UA-64, National Aeronautical Establishment, NRC, Canada, January 1983.

7. Reyers, M. E., Kapoor, K. B., and Moulton, B. E., "Pitch- and Yaw-Oscillation Experiments on the Standard Dynamics Model at Mach 0.6," Report LTR-UA-76, National Aeronautical Establishment, NRC, Canada, June 1984.

8. Barnhart, B., "F-15 Rotary Balance Data for an Angle-of-Attack Range of 8 Deg to 90 Deg," NASA Contractor Report 3478, May 1982, Prepared for NASA Langley Research Center by Bihrle Applied Research, Inc.

9. Jermey, C. and Schiff L. B., "Aerodynamic Characteristics of Standard Model in Coning Motion at Mach 0.6," proposed NASA TM-86717.

Fig. 1. Model and apparatus on laboratory test stand.

Fig. 2. Model and apparatus in 12-Foot Pressure Wind Tunnel.
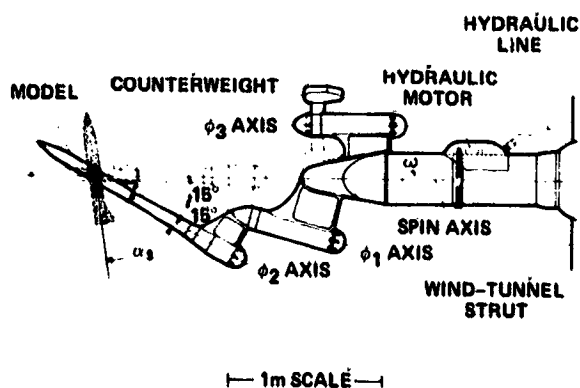
Fig. 3. Large-scale rotary-balance apparatus.
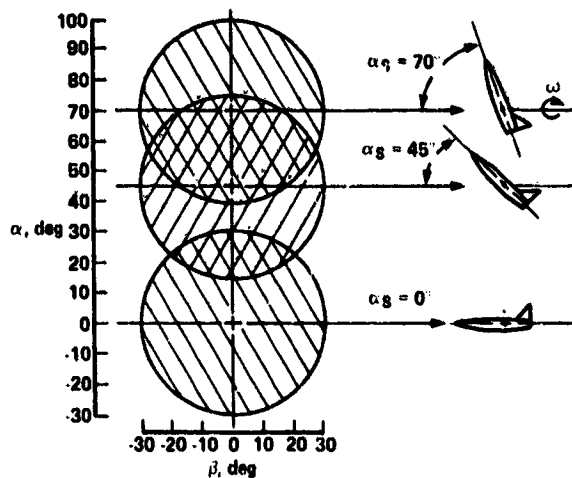
Fig. 4. Attitude envelope for large-scale rotary-balance apparatus.

10

Fig. 5. F-15 model mounted on various stings. (a) $\alpha_s = 0°$. (b) $\alpha_s = 45°$. (c) $\alpha_s = 70°$.
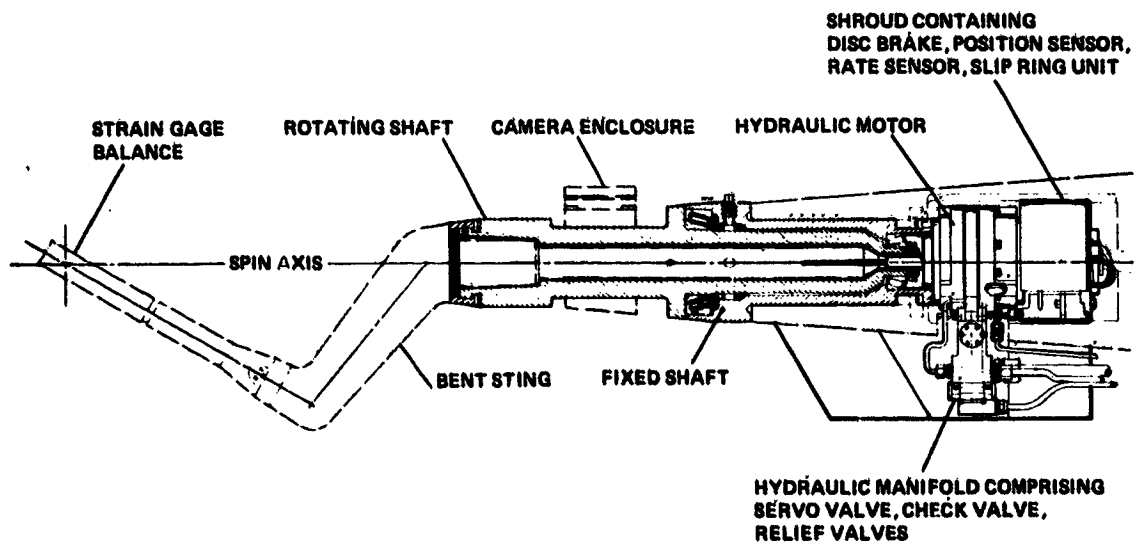
Fig. 6. Small-scale rotary-balance apparatus.

11

Fig. 7. Standard Dynamics Model on 30° bent sting in 6- by 6-Foot Supersonic Wind Tunnel.
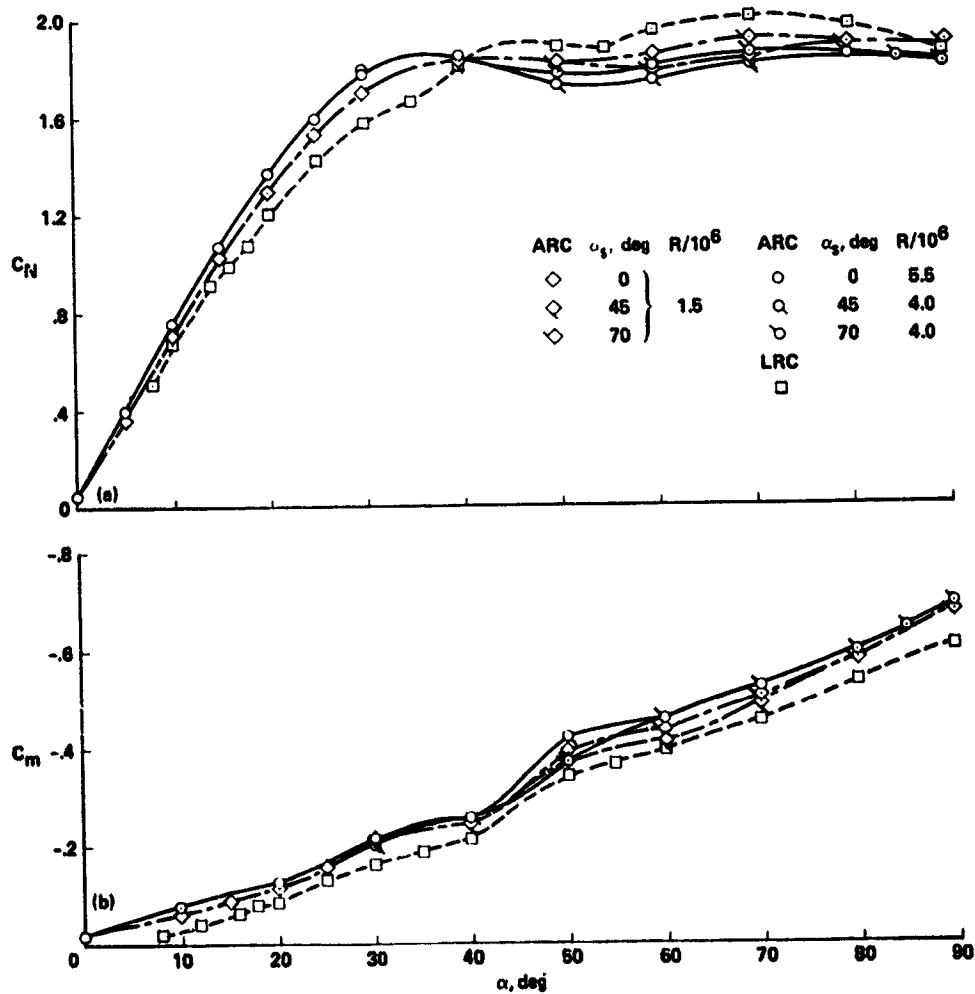
Fig. 8. Effect of Reynolds number on the longitudinal aerodynamic coefficients for the F-15, nose boom off. (a) Normal-force coefficient. (b) Pitching-moment coefficient.

12
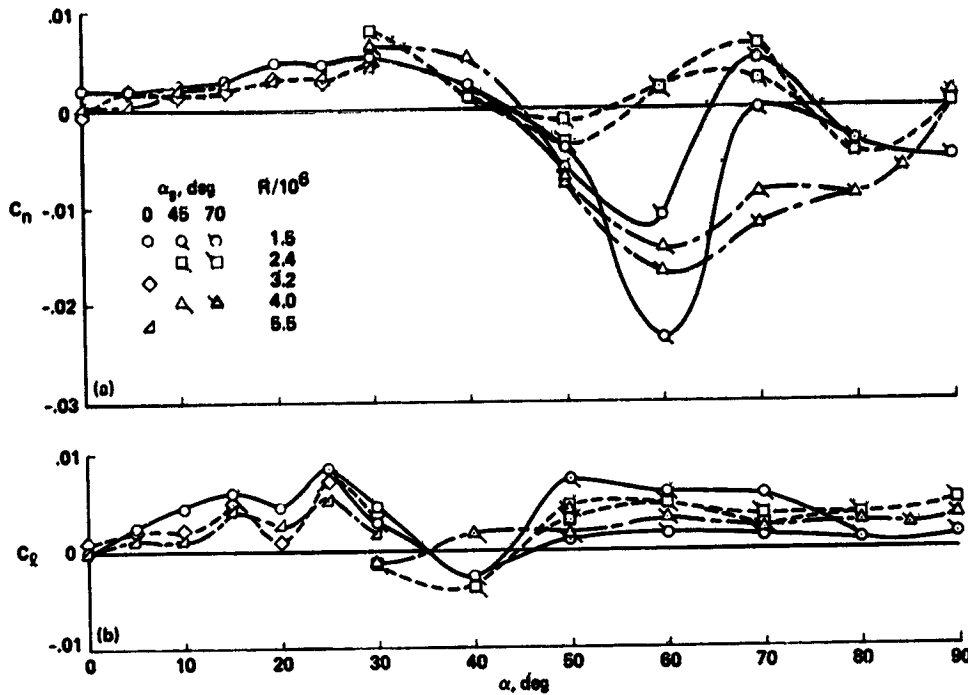
Fig. 9. Effect of Reynolds number on the lateral-directional aerodynamic coefficients for the F-15, nose boom off. (a) Yawing-moment coefficient. (b) Rolling-moment coefficient.
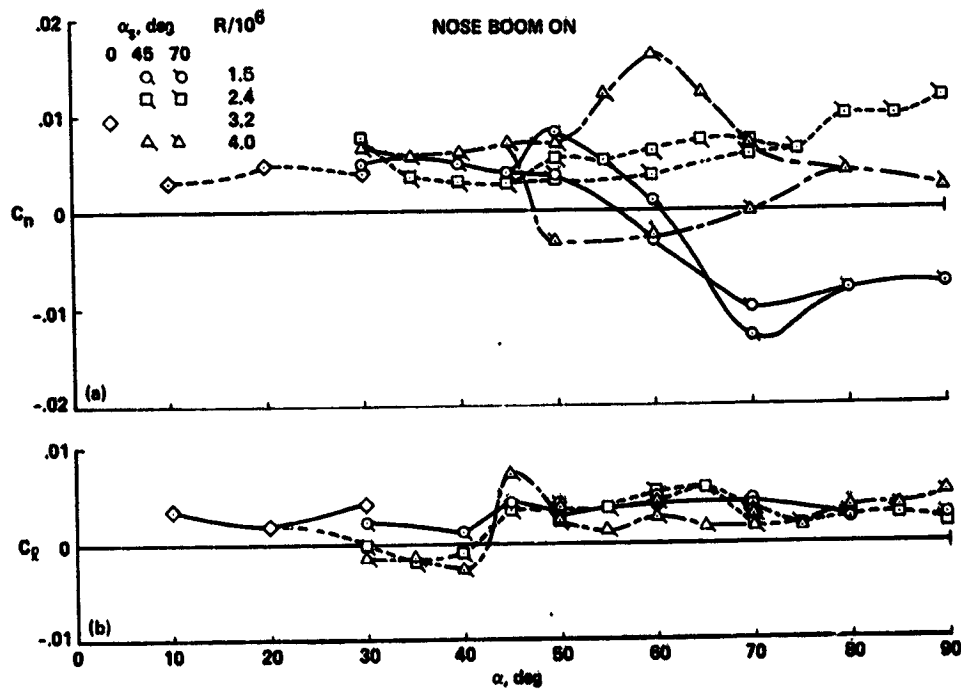
Fig. 10. Effects of Reynolds number on the lateral-directional aerodynamic coefficients for the F-15, nose boom on. (a) Yawing-moment coefficient. (b) Rolling-moment coefficient.
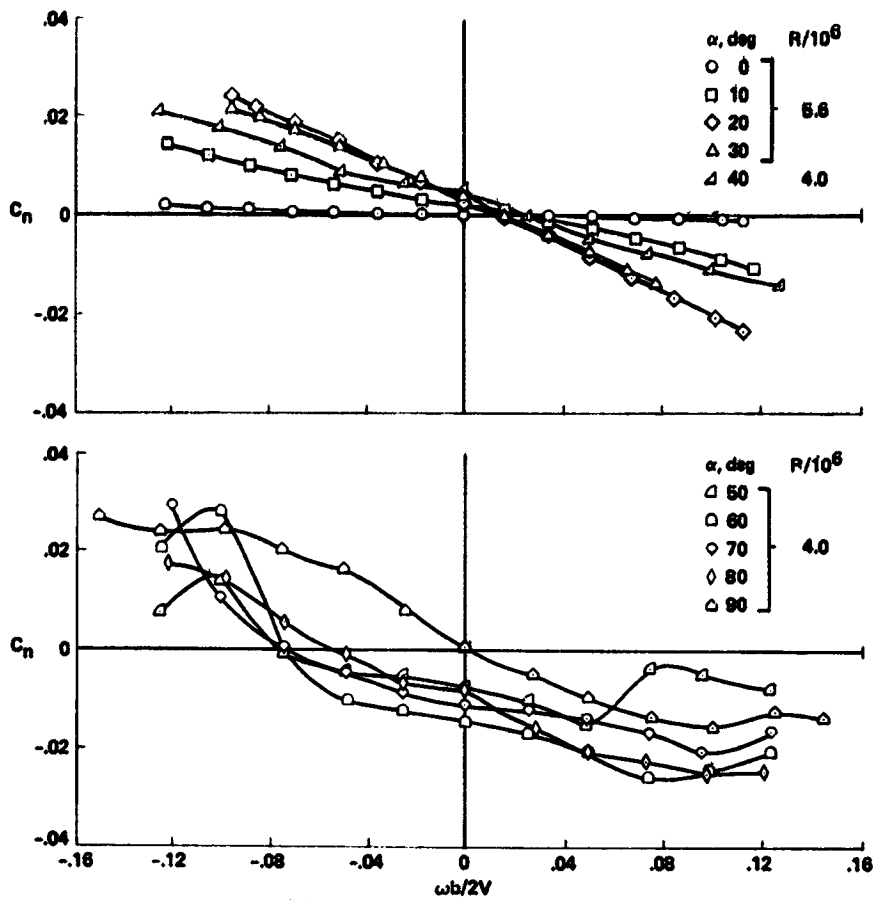
(a) Yawing-moment coefficient.
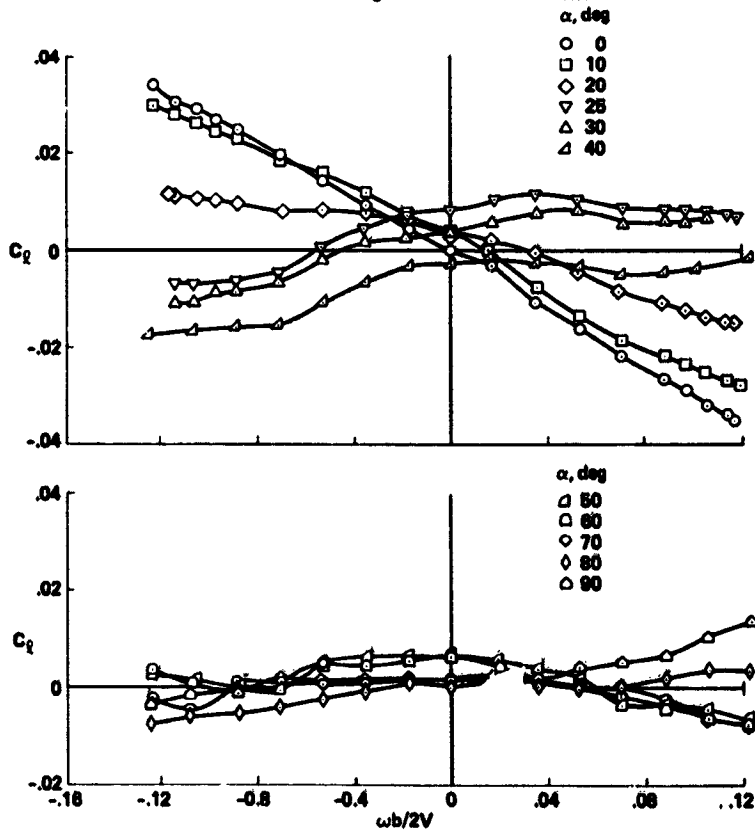
(b) Rolling-moment coefficient.

Fig. 11. Effects of rotation rate and angle of attack on the lateral-directional aerodynamic coefficients for the F-15, nose boom off, R = 1.5 million.

14

(a) Yawing-moment coefficient.

(b) Rolling-moment coefficient.
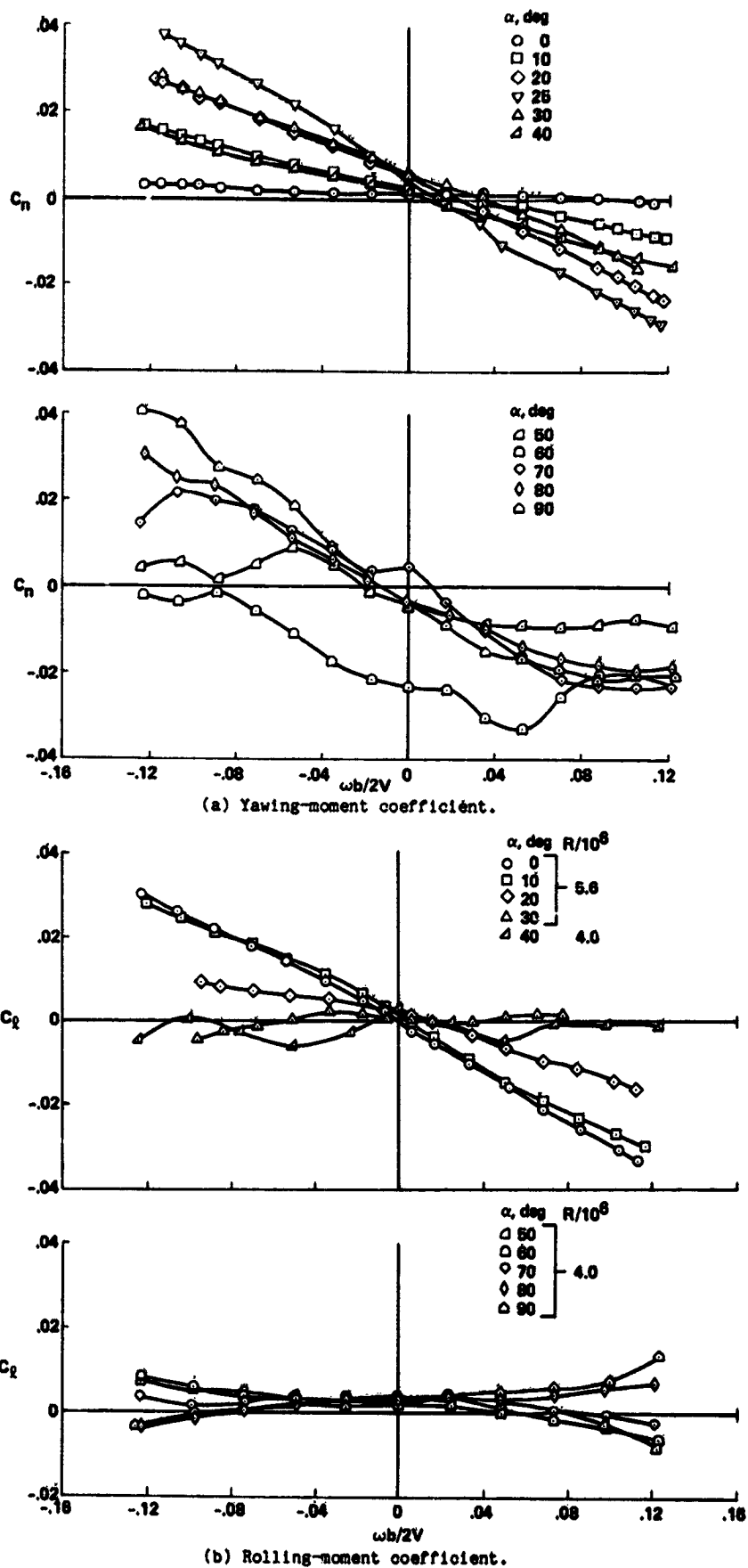
Fig. 12. Effects of rotation rate and angle of attack on the lateral-directional aerodynamic coefficients for the F-15, nose boom off, R = 4.0 and 5.6 million.
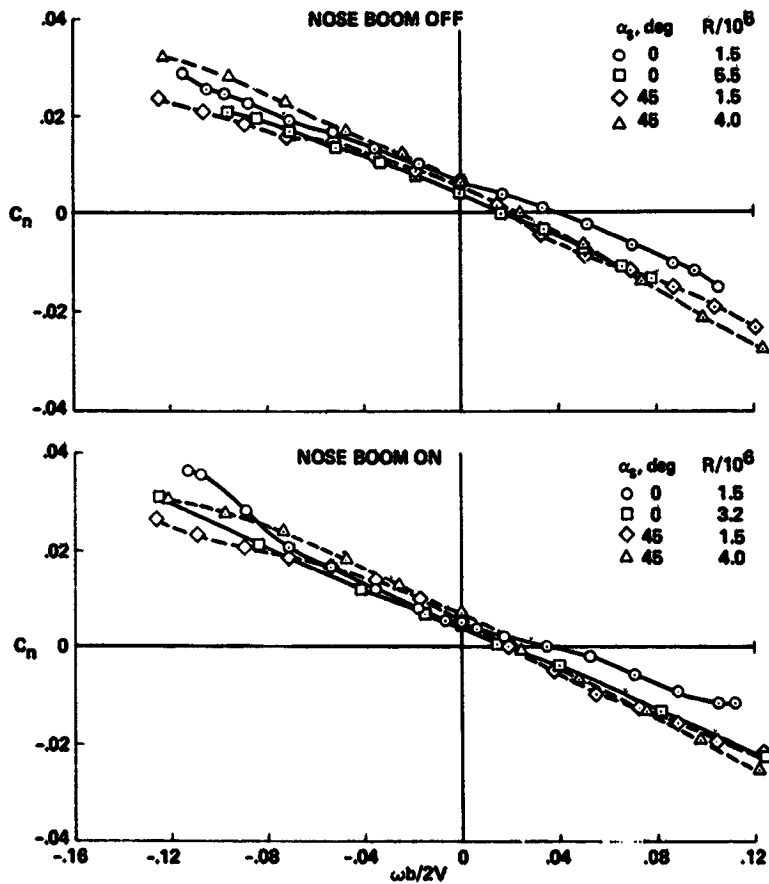
Fig. 13. Effects of rotation rate and sting angle on the yawing-moment coefficient for the F-15 at α = 30°. (a) Nose boom off. (b) Nose boom on.
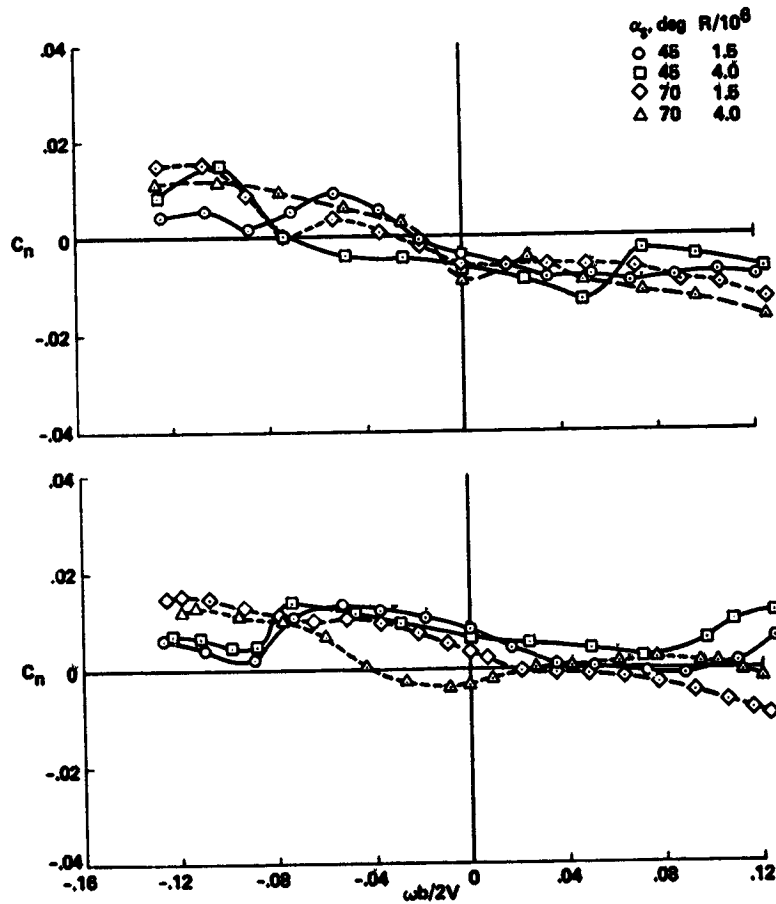
Fig. 14. Effects of rotation rate and sting angle on the yawing-moment coefficient for the F-15 at
α = 50°. (a) Nose boom off. (b) Nose boom on.
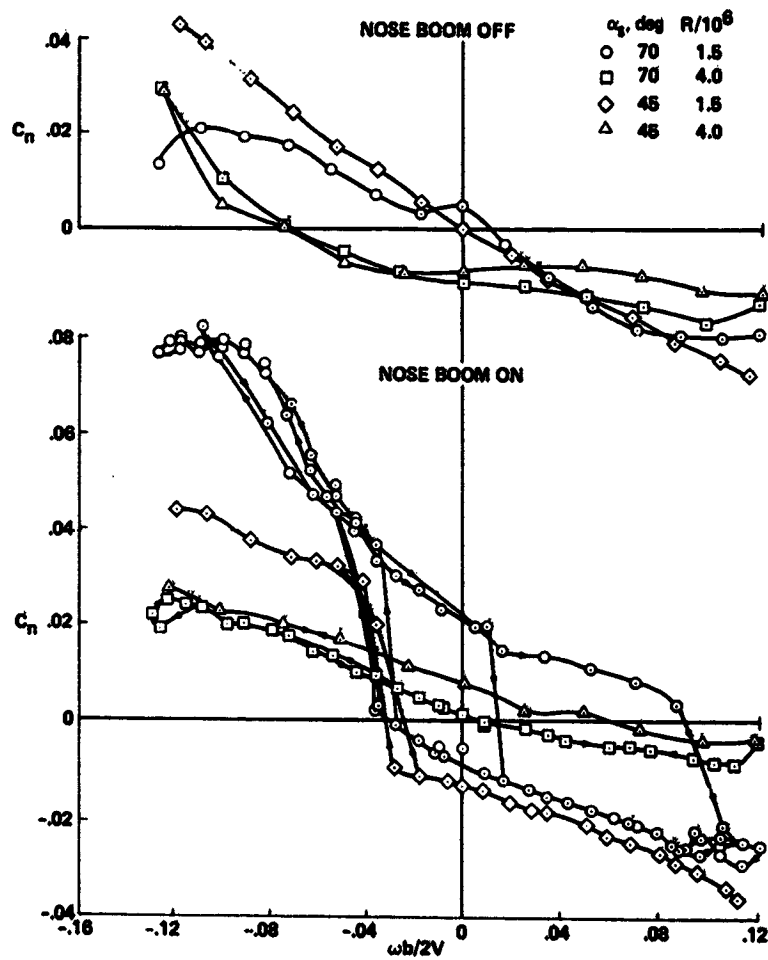
Fig. 15. Effects of rotation rate and sting angle on the yawing-moment coefficient for the F-15 at
$\alpha = 70°$. (a) Nose boom off. (b) Nose boom on.
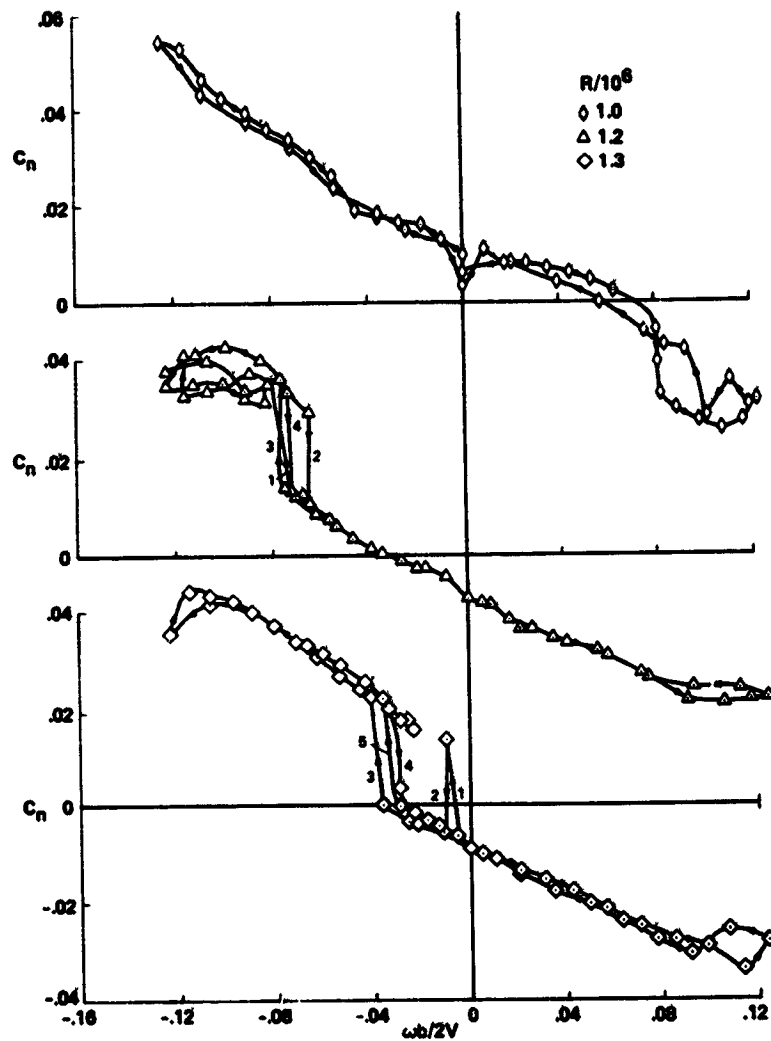
Fig. 16. Effects of rotation rate and Reynolds number on the yawing-moment coefficient for the F-15, nose boom on, $\alpha_B = 70°$, $\alpha = 70°$.
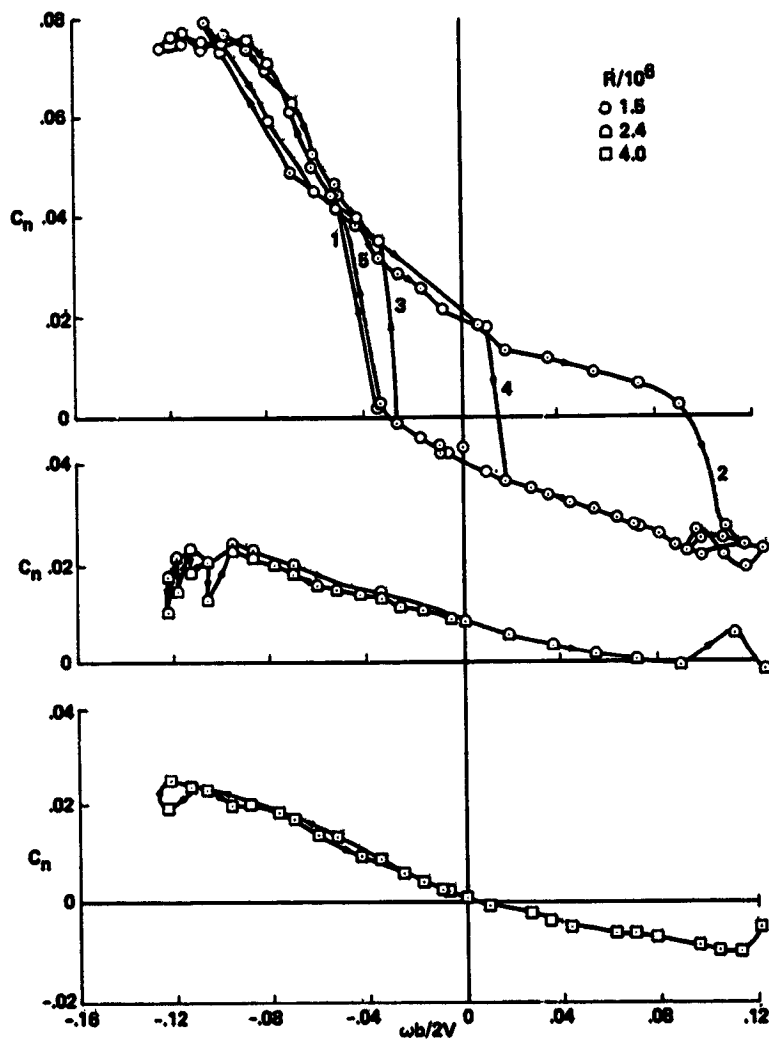
Fig. 16. Concluded.
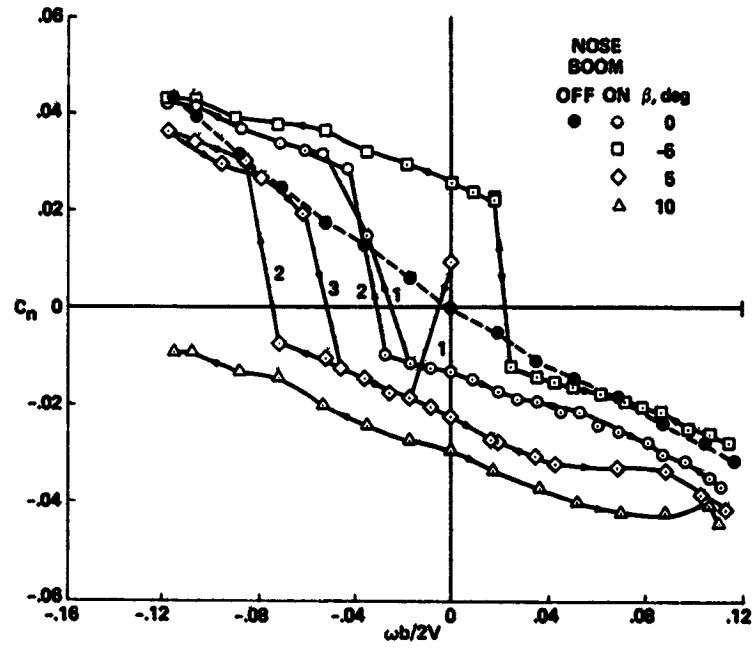
Fig. 17. Effects of rotation rate and sideslip angle on the yawing-moment coefficient for the F-15, $\alpha = 70°$, $\alpha_s = 45°$, $R = 1.5$ million.

(a) α = 10°.
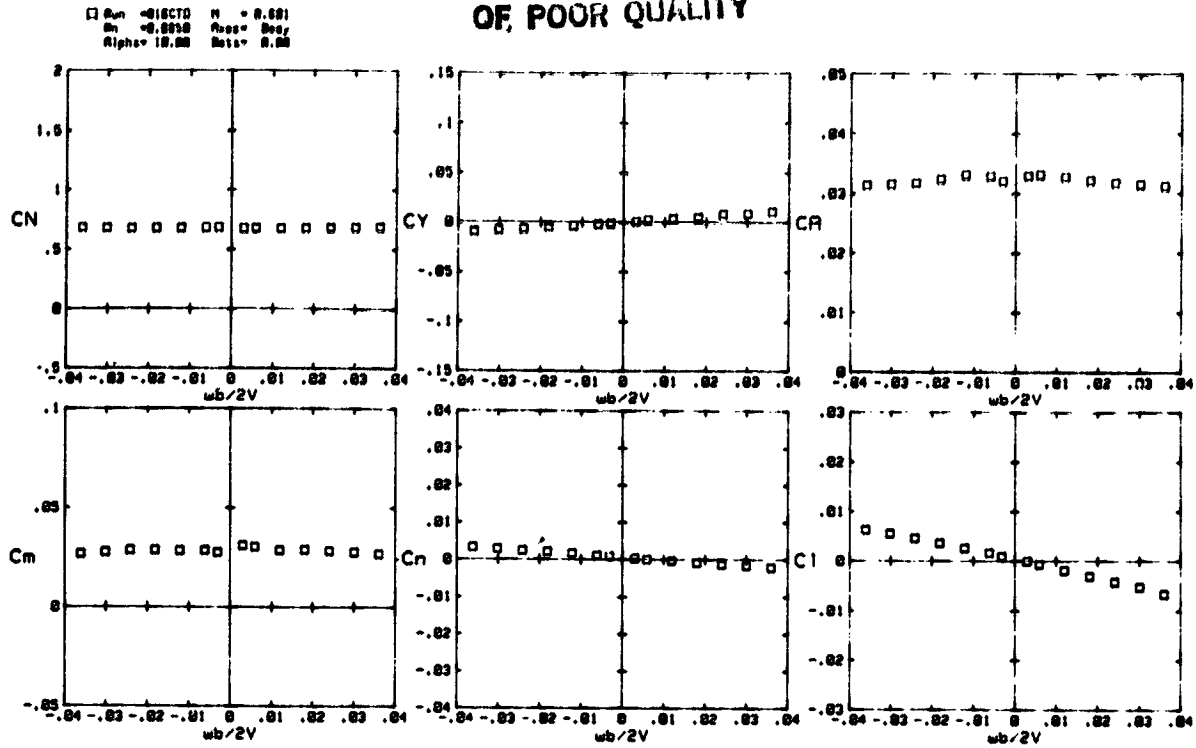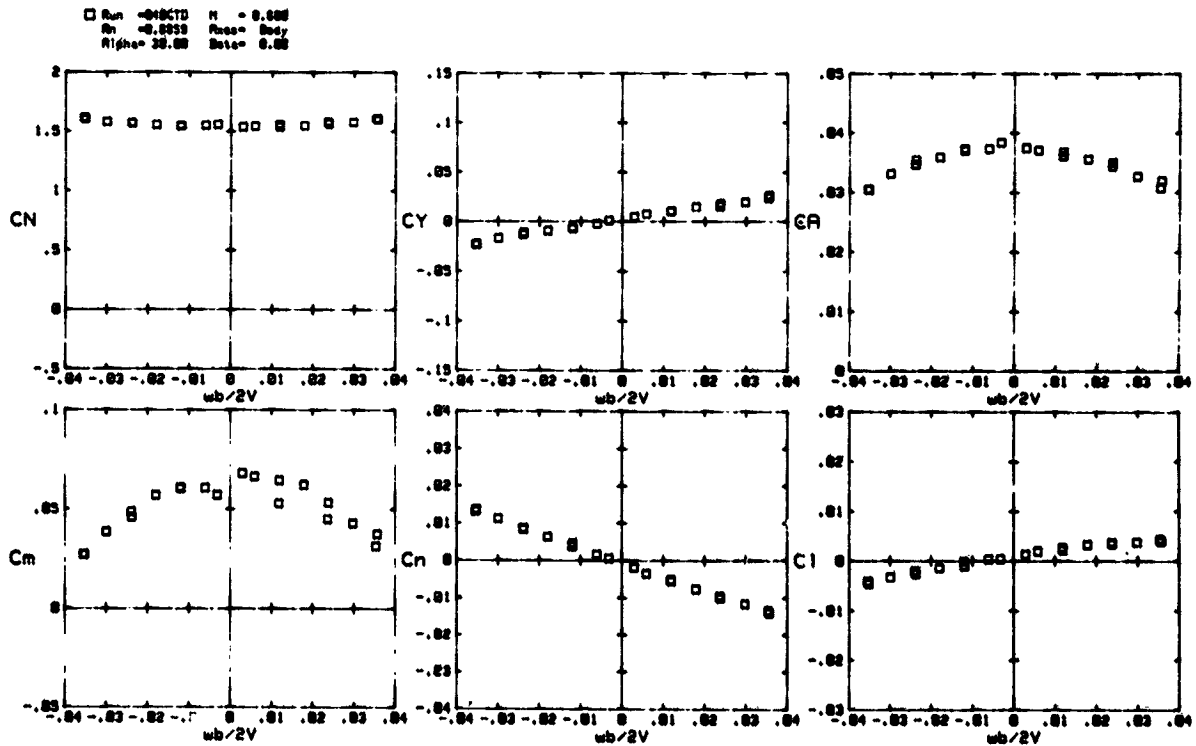
(b) α = 30°.

Fig. 18. Effect of rotation rate on aerodynamic coefficients for Standard Dynamics Model at β = 0°.

(a) α = 10°.
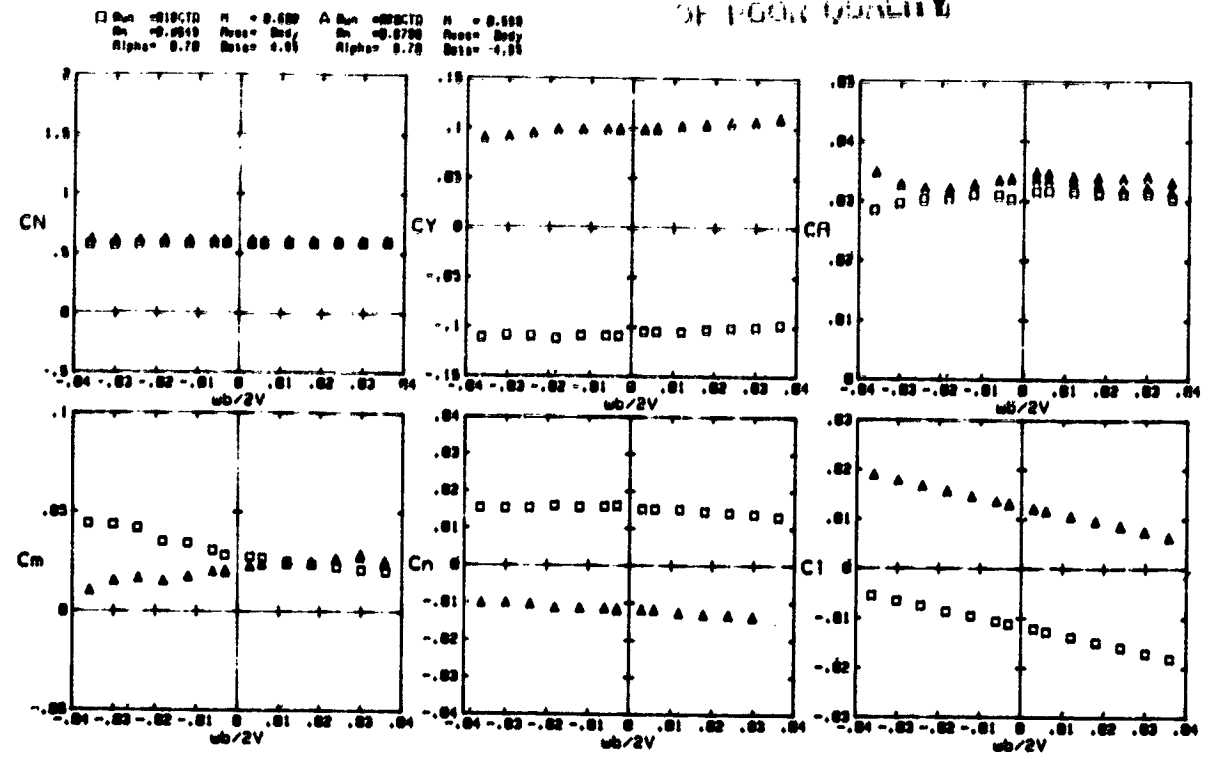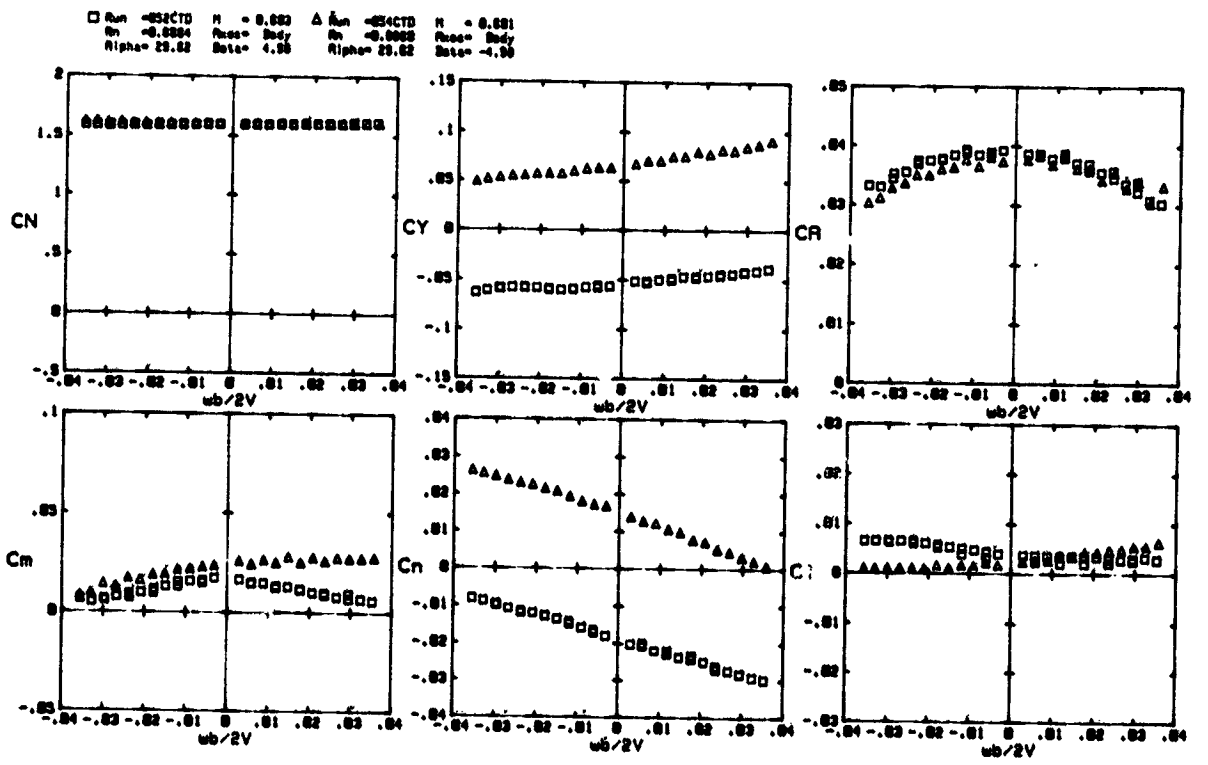
(b) α = 30°.

Fig. 19. Effect of rotation rate on aerodynamic coefficients for Standard Dynamics Model at β = +5° and -5°.
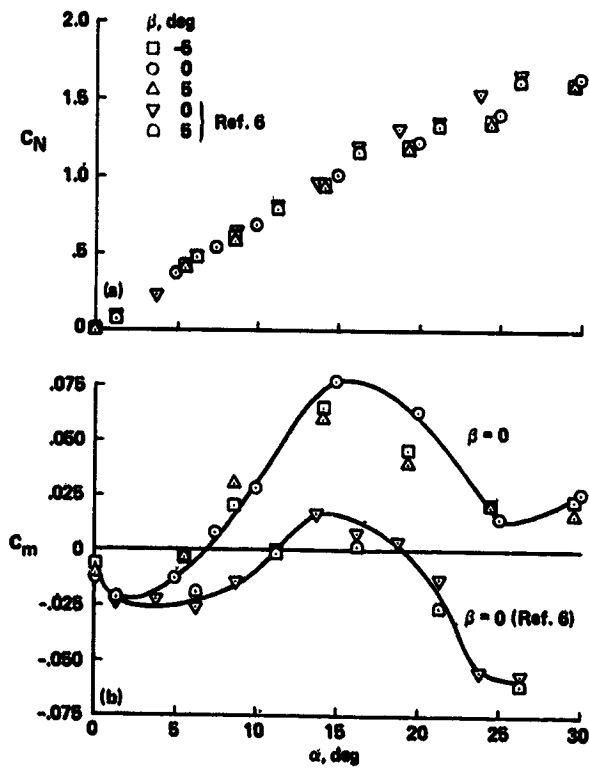
Fig. 20. Longitudinal aerodynamic coefficients
for Standard Dynamics Model. (a) Normal-force
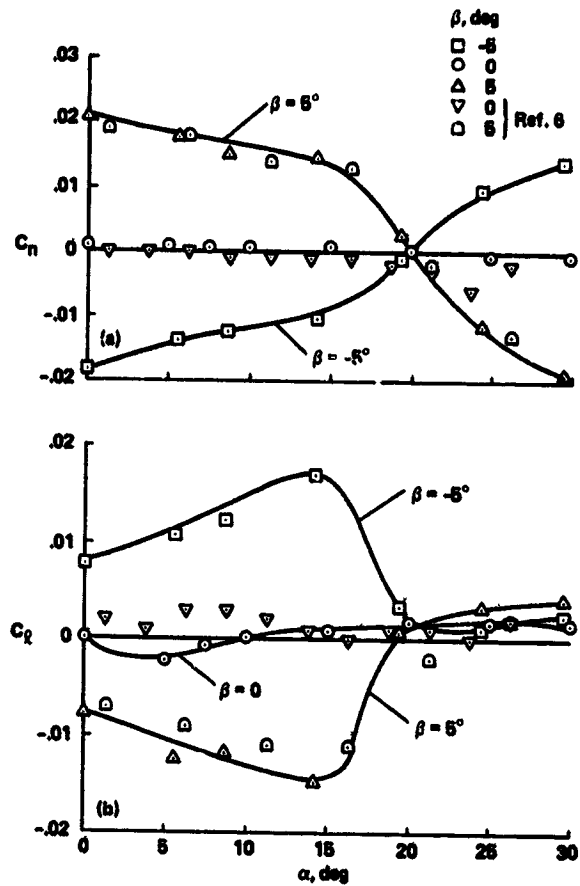coefficient. (b) Pitching-moment coefficient.

Fig. 21. Lateral-directional aerodynamic
coefficients for Standard Dynamics Model.
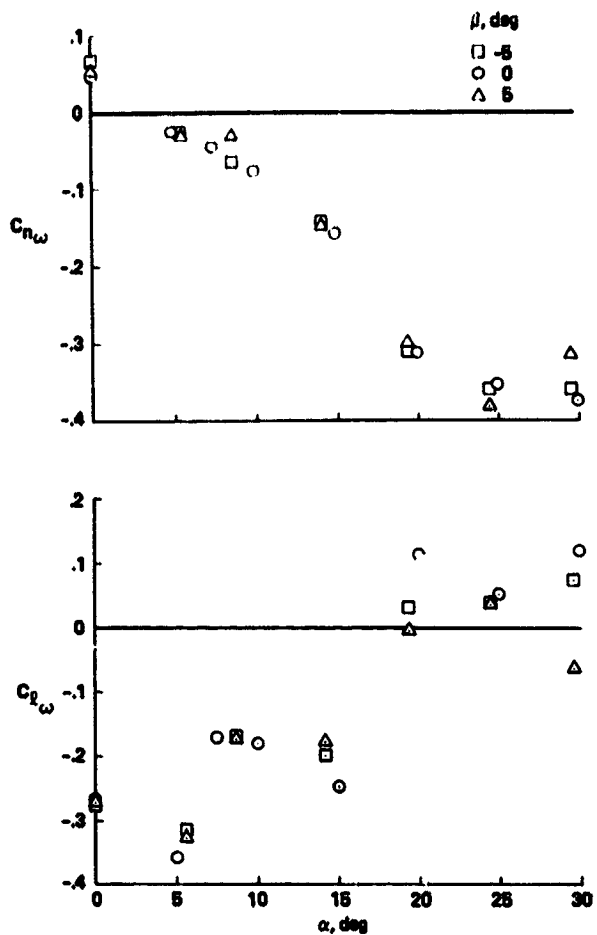(a) Yawing-moment coefficient. (b) Rolling-
moment coefficient.

Fig. 22. Variation of lateral-directional rotary derivatives with angle of attack for Standard Dynamics Model. (a) Yawing-moment derivative. (b) Rolling-moment derivative.

1. Report No. NASA TM-86714	2. Government Accession No.	3. Recipient's Catalog No.	
4. Title and Subtitle RECENT DEVELOPMENT IN ROTARY-BALANCE TESTING OF FIGHTER AIRCRAFT CONFIGURATIONS AT NASA AMES RESEARCH CENTER		5. Report Date July 1985	
		6. Performing Organization Code	
7. Author(s) Gerald N. Malcolm and Lewis B. Schiff		8. Performing Organization Report No. 85211	
		10. Work Unit No. 505-43-11	
9. Performing Organization Name and Address Ames Research Center Moffett Field, CA 94035		11. Contract or Grant No.	
		13. Type of Report and Period Covered Technical Memorandum	
12. Sponsoring Agency Name and Address National Aeronautics and Space Administration Washington, D.C. 20546			
		14. Sponsoring Agency Code	

15. Supplementary Notes

Point of Contact: Gerald N. Malcolm, Ames Research Center, MS 227-6
Moffett Field, CA 94035
(415) 694-6208 or FTS 464-6208

16. Abstract

NASA Ames Research Center has an ongoing research program to investigate high-angle-of-attack aerodynamic phenomena associated with high-performance aircraft. As part of this research effort, two rotary-balance apparatuses have recently been developed for testing airplane models in a coning motion. A new large-scale apparatus, developed for use in the 12-Foot Pressure Wind Tunnel primarily to permit testing at high Reynolds numbers, was recently used to investigate the aerodynamics of 0.05-scale model of the F-15 fighter aircraft. Effects of Reynolds number, spin-rate parameter, model attitude, presence of a nose boom, and model/sting mounting angle were investigated.

A smaller apparatus, which is a modernized version of a coning rig developed several years ago to investigate the aerodynamics of bodies of revolution in a coning motion, has been used in the 6- by 6-Foot Supersonic Wind Tunnel to investigate the aerodynamic behavior of a simple representation of a modern fighter, the Standard Dynamic Model (SDM). Effects of spin-rate parameter and model attitude were investigated. A description of the two rigs and a discussion of some of the results obtained in the respective test are presented.

17. Key Words (Suggested by Author(s)) Rotary-balance testing High angle of attack	18. Distribution Statement Unlimited Subject Category - 01		
19. Security Classif. (of this report) Unclassified	20. Security Classif. (of this page) Unclassified	21. No. of Pages	22. Price